PHYSICAL REVIEW B VOLUME 49, NUMBER 24 15 JUNE 1994-II

Trigonal gold-pair center in silicon

A. Thilderkvist, S. Ghatnekar Nilsson, M. Kleverman, and H. G. Grimmeiss
Department of Solid State Physics, University of Lund, Box 118, S-221 00 Lund, Sweden

(Received 25 February 1994)

The electronic and vibrational properties of a gold-related center in silicon have been studied by Fourier-transform spectroscopy using uniaxial stress and Zeeman spectroscopy. Thirteen different characteristic line series have been identified, of which 11 consist of a relatively intense zero-phonon line followed by several phonon replicas. The line series are assigned to internal transitions at a gold-related center in two different charge states, i.e., the neutral and negatively charged states for which the phonon energy is about 119.8 and 105.7 cm^{-1}, respectively. A Huang-Rhys factor of 1.4 ± 0.1 was determined for the $\hbar\omega = 119.8$ cm^{-1} series. The center has trigonal symmetry deduced from uniaxial stress and Zeeman experiments. A dissociation energy of about 1.7 eV was determined from an isothermal annealing study. The trigonal symmetry and the high dissociation energy strongly suggest that the center consists of two nearest-neighbor substitutional gold atoms. A divacancy model is employed that makes a qualitative understanding of the electronic properties of the center possible.

I. INTRODUCTION

The electronic structure of gold-related deep centers in silicon has attracted a great amount of interest and then especially the well-known acceptor and donor levels at $E_v+0.35$ eV and $E_v+0.67$ eV, respectively.[1-4] Sharp line spectra of these levels have been studied in some detail.[3,5,6] It has been shown that the acceptor and donor spectra belong to the same gold center and, based on several studies,[3,7] most probably the single substitutional gold center.

In this paper, the interest is focused on additional lines in the energy range from 5000 to 8700 cm^{-1} that are always observed in our gold-doped silicon samples. Recently,[8] we discussed some preliminary results for this spectrum of lines which then were grouped into 12 different series with similar spectral features. All series consist of a zero-phonon line followed by a number of approximately equally spaced phonon replicas. Three of the most intense series were first reported by Ohta[9] who suggested that they are all due to internal transitions at the same gold complex consisting of two gold atoms, i.e., a gold-pair center. Ohta estimated the dissociation energy of the gold complex to be in the range 0.6–1.2 eV which indicates that the center consists of two substitutional atoms. The internuclear distance in the free gold molecule exceeds the nearest-neighbor silicon distance which lead Ohta to suggest that the Au atoms were located at the second-nearest substitutional sites resulting in a rhombic I symmetry (C_{2v}) for the center. However, this was clearly in disagreement with our preliminary uniaxial stress and Zeeman results[8] that unambiguously showed that the center has trigonal symmetry. A trigonal symmetry strongly indicates that the Au atoms are on nearest-neighbor lattice sites.

In this paper, results from high-resolution measurements are reported which facilitate a detailed analysis of the electronic and vibrational structure of the gold-pair center. The symmetry of the initial state and some of the final states of the excitation spectra have been identified from uniaxial stress and Zeeman measurements. Results from doping and isothermal annealing experiments are reported. The experimental results are examined by employing a one-particle divacancy model including spin-orbit, (*s*-*o*), and Coulomb interaction. A qualitative and, to some extent, a quantitative understanding of the electronic structure of the gold-pair center is obtained.

II. EXPERIMENTAL DETAILS

Au-doped samples were prepared from *p*- or *n*-type silicon substrates (boron- or phosphorus-doped) having resistivies ranging from 0.09 Ω cm to 250 Ω cm. The samples were lapped, polished, and etched in $HF+H_2O$. A gold layer with a thickness of approximately 300 nm was then evaporated. The samples were introduced into quartz ampoules which were evacuated and sealed off. A heat treatment at about 1250 °C for 16 h was carried out followed by a rapid quench to room temperature by dropping the samples in ethylene glycol. Ohmic contacts used for photoconductivity (PC) measurements were obtained by rubbing Al-Ga onto parts of the surface. Samples for unaxial stress measurements, oriented in the $\langle 001\rangle$, $\langle 110\rangle$, or $\langle 111\rangle$ directions, had a geometry of about $2\times2\times8$ mm^3. The end surfaces were either lapped parallel or lapped into a pyramidal shape in order to achieve homogeneous stress.

The spectra were recorded with a BOMEM DA 3.01 Fourier-transform spectrometer, equipped with a nitrogen-cooled In:Sb detector. In the Zeeman experiments, an Oxford SM-4 split-coil magnet in the Voigt configuration was used and the sample temperature was kept at about 2 K. The maximum field used was 6.3 T. In the stress measurements the samples were mounted in a stress rig and were exposed to uniaxial stress through a push rod and pressurized air. The temperature of the

0163-1829/94/49(24)/16926(16)/$06.00

sample was kept at about 10 K in a liquid-helium continuous-flow cryostat.

III. EXPERIMENTAL RESULTS AND DISCUSSION

A. Nonperturbation data

In Fig. 1(a) an overall transmission spectrum obtained from an originally 250 Ω cm *n*-type gold-doped sample is presented. Several different series of sharp lines are clearly observed. The Au acceptor and donor spectra at about 5000 and 6400 cm^{-1}, respectively, are identified by comparison with previous results.[1-8] As is observed, a wealth of spectral features remain to be analyzed in more detailed. However, we focus our attention only on the series of line spectra identified by their corresponding zero-phonon lines $A_0, B_0, \ldots, F_0$ in Fig. 1(a). With reference to Fig. 1(a), five phonon replicas are clearly resolved for the *A* series. A closer inspection reveals two additional series (A' and A'') near the *A* series and they are shown in Fig. 2. Both the A' and A'' series have a relatively low intensity but their connections with the other series are unambiguous since also their first phonon replicas are clearly observed. The A' series has been reported by us previously,[8] whereas the A'' series hitherto has been overlooked. In the energy range between 6600 and 7000 cm^{-1} five series of lines are observed and they are denoted *B*, *C*, *D*, and *E*, respectively. Finally, at about 8100 cm^{-1}, a series of considerably broader lines is found and it is labeled *F*, accordingly. Already at a first glance on the line spectra in Fig. 1(a) it becomes clear that all eight line series have very similar structure and, therefore, must be due to excitation of the same center. In Table I the phonon energies for the eight series obtained by a linear regression analysis of the experimental data are presented. All phonon energies are almost identical which gives a final proof of the common origin of the series. A mean value of about $\hbar\omega = 119.8$ cm^{-1} was deduced for the phonon energy.

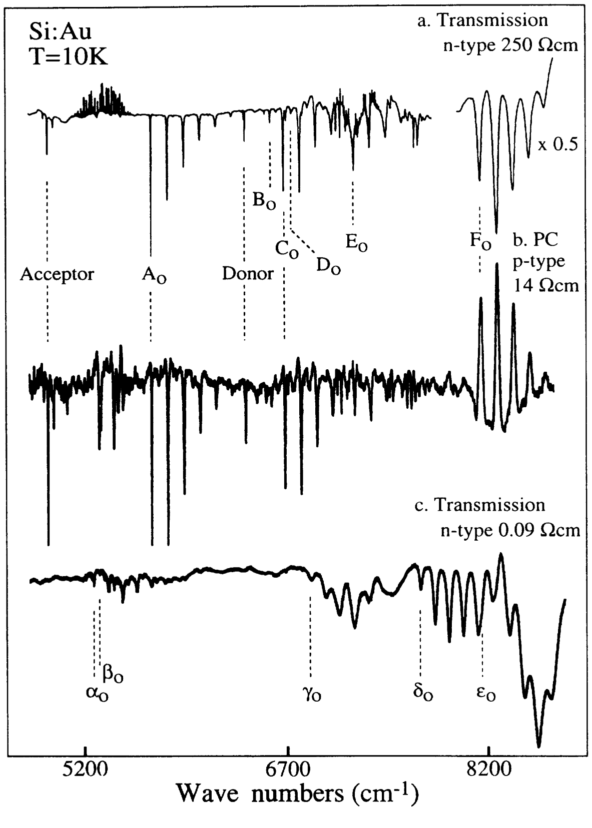

FIG. 1. Three overall spectra obtained from Au-doped silicon samples. In (a) a transmission spectrum from originally *n*-type, 250 Ω cm, silicon is shown. The Au acceptor and donor are marked in the figure as well as the zero-phonon lines for the series *A*–*F*. (b) shows a photoconductivity spectrum from originally *p*-type, 14 Ω cm, silicon. The spectral lines marked in (a) are easily identified also in this spectrum. In (c) a transmission spectrum from originally *n*-type, 0.09 Ω cm, silicon is presented where the zero-phonon lines of the α to ε series are indicated.

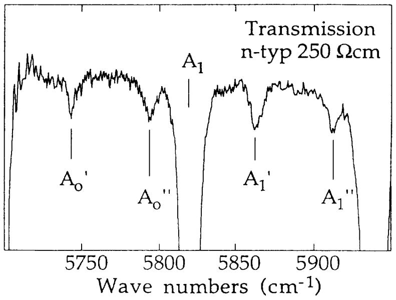

FIG. 2. A blow up of the transmission spectrum from originally *n*-type, 250 Ω cm, silicon in the energy range 5700–5950 cm^{-1}. The A' and A'' series are indicated as well as the first phonon replica of the *A* series.

To obtain additional information, PC experiments were carried out on an originally 14 Ω cm *p*-type gold-doped sample. A typical PC spectrum is presented in Fig. 1(b). By inspection, clearly the transmission and PC spectrum in Fig. 1(a) and 1(b) respectively, show close similarities. However, the line series *A*-*E* give rise to a negative PC signal, whereas the *F* series contributes positively. In a PC measurement only those optically excited charge carriers that enter a band can contribute positively to the current. The sharp PC line spectrum presented in Fig. 1(b) is superimposed on an intense background signal which gives rise to a relatively high current detected in the external circuit. The negative PC signal observed for the *A*-*E* series may then be understood by considering that when a final state in the excitation is within the band gap, photons may be absorbed but no charge carries enter the band. The transitions are thus observed as dips in the background signal since photons are stolen from the background process which would result in free charge carriers.

If the final state is resonant with a band continuum, a broadening of the excitation line is expected due to interaction between the discrete state and the continuum. A charge carrier in the resonant quasidiscrete state has two main deexcitation paths. The first one involves a direct capture to a bound state in the band gap and, hence, no contribution to the PC current is expected. The second one is that the charge carrier leaks out into the continuum irreversibly and, consequently, a contribu-

TABLE I. The phonon energies for the series *A*-*F*, given in wave numbers (cm^{-1}). The phonon energies for each series obtained from a linear fit to the experimental data are listed in the last column. For comparison the results of Ohta (Ref. 9) for the series *A*, *C*, and *F* are listed in the last three rows of the table.

Series (cm^{-1})	$n=0$	$n=1$	$n=2$	$n=3$	$n=4$	$n=5$	$\hbar\omega$ (cm^{-1})
A	5699.4	5819.9	5939.6	6058.6	6177.1	6294.7	119.1
A'	5743	5863	5982				120
A''	5792	5913	6031				120
B	6589.2	6710.1	6830.4	6951.2			120.6
C	6688.9	6809.8	6929.9	7048.1	7168.7		119.8
D	6746.8	6867.3	6987.1				120.1
E	7212.0	7332.3	7452.1	7571.0			119.7
F	8147.1	8266.6	8385.9	8503.2	8623.2		118.9
A	5700	5823	5945	6062	6182		
C	6693	6807	6936	7056			
F	8155	8275	8394	8512	8630	8749	

tion to the current is obtained. Depending on the relative strengths of these two processes as well as the strength of the background signal, both positive and negative peaks (resonances) may be observed. The considerable broadening observed both in the transmission and PC spectra for the lines in the *F* series, and the positive PC signal, strongly indicates that the final states are to be found as resonances in a band continuum.

The relative intensities among the eight line series $A, B, \ldots, F$ remain constant in samples with different background doping. However, the total intensity of these series decrease in samples made of originally highly *n*-doped material, whereas several new line series increase in intensity. In Fig. 1(c), a transmission spectrum obtained in an originally 0.09 Ω cm *n*-type sample is presented. Five new series labeled α, β, γ, δ, and ε are observed, and they show the same characteristic features with a zero-phonon line followed by several phonon replicas, as was observed for the *A*-*F* series. The zero-phonon lines $\alpha_0, \beta_0, \ldots, \varepsilon_0$ are marked in the figure. The phonon energy of the new series (see Table II) is somewhat lower compared to that of the *A*-*F* series with a mean value of about $\hbar\omega = 105.7\ \mathrm{cm}^{-1}$. An obvious explanation to these observations is that the center could be observed in two different charge states, i.e., the neutral and the negatively charged states.

A total of 13 series of lines are thus observed and the photon energies for the *A*-*F* and α-ε series as well as the phonon energies are listed in Tables I and II, respectively. Also included in Table I are the results obtained by Ohta for the most intense series *A*, *C*, and *F*. The energies obtained in this work differs slightly from those of Ohta but our assignment of his lines according to our notations is unambiguous.

The relative integrated intensity and the FWHM (full width at half maximum) of the zero-phonon lines of the *A*-*F* series were also measured and are presented in Table III. The relative intensity of the lines within a given series is a measure of the electron-phonon interaction which can be described by the Huang-Rhys factor *S*. For a one-dimensional oscillator the intensity for a transition from the electronic ground state in its lowest phonon state to the *n*th phonon state of the electronic final state can be written.

$$I_{0n} \propto \frac{S^n}{n!} e^{-S} , \tag{1}$$

where *n* is the number of phonons in the final state. The intensities of the lines in the series *A*, *C*, and *F* are normalized to the strongest line ($n=1$) and are plotted as a function of *n* in Fig. 3. Also shown in this figure is a fit of Eq. (1) to the data, which results in a mean value for the three series of $S = 1.4 \pm 0.1$. This value is in good agreement with the result by Ohta who deduced $S = 1.6 \pm 0.2$ for the series *A*, *C*, and *F*.

In the case of the *A* series, the phonon replicas are

TABLE II. The photon energies for the series α-ε, given in wave numbers (cm^{-1}). The photon energies obtained from a linear fit to the experimental data are given in the last column.

Series (cm^{-1})	$n=0$	$n=1$	$n=2$	$n=3$	$n=4$	$n=5$	$n=6$	$\hbar\omega$ (cm^{-1})
α	5263.8	5371.8	5478.8	5584.9	5691.4	5797.0	5900.2	106.2
β	5304.3	5412.8	5518.4	5625.4	5732.4	5836.1		106.4
γ	6995.7	7092.9	7203.7	7313.3				106.4
δ	7695.2	7801.7	7906.7	8013.2	8116.7	8221.6		105.2
ε	8144.9	8245.1	8357.0	8460.4	8562.3	8659.4	8774.5	104.4

TABLE III. Intensities and FWHM for the zero-phonon lines of the *A*-*F* series as well as for the A_0' and A_0'' lines. The intensities are normalized to the A_0 line. Also included are the symmetries of the final states, Γ_f, deduced from uniaxial stress, Zeeman, and polarization experiments, where * indicates the tentative assignment from the divacancy model.

Lines:	A_0	B_0	C_0	D_0	E_0	F_0	A_0'	A_0''
Intensity	1.0	0.4	2.0	0.3	1.1	38	0.02	0.02
FWHM (cm^{-1})	1.1	5.2	4.1	13.1	6.7	34	3	5.4
Γ_f	E_u	A_{1u}^*	A_{2u}	A_{1u}^*	A_{2u}^*	E_u^*		

reasonably sharp and their energy positions could be measured with high accuracy. This makes the *A* series suitable for a more detailed analysis of the phonon replicas. It was found that the phonon energy was not constant but decreases with increasing phonon quantum number *n*. This could be a result of anharmonicity in the oscillator potential. Assuming the oscillator to be one dimensional and that the leading anharmonicity term is $H'=\sigma\hbar\omega Q^3$, where Q is the configuration coordinate, the phonon energy varies according to[10]

$$E_n=\hbar\omega[(n+\tfrac{1}{2})-\tfrac{15}{4}\sigma^2(n+\tfrac{1}{2})^2-\tfrac{7}{16}\sigma^2] \ . \qquad (2)$$

In Fig. 4 (E_n-E_{n-1}) is plotted versus n for the *A* series. According to Eq. (2), the slope is given by $-(15/2)\sigma^2\hbar\omega$ which results in an anharmonicity constant of $\sigma=2.8\times10^{-2}$.

B. Uniaxial stress

Transmission spectroscopy in conjunction with uniaxial stress of the zero-phonon lines allows for studies of the symmetry and the electronic structure of the defect center. When a silicon crystal is subjected to uniaxial stress the point-group symmetry is lowered and degeneracies may be lifted. In the case of axial centers, all possible orientations of the centers are equivalent at zero stress and, hence, have the same energy. Under stress this equivalence may no longer prevail and centers oriented nonequivalently with respect to the stress axis may shift in energy differently. In addition, the electronic states involved in the transitions may be degenerate at zero stress and this electronic degeneracy may also be lifted by the applied stress.

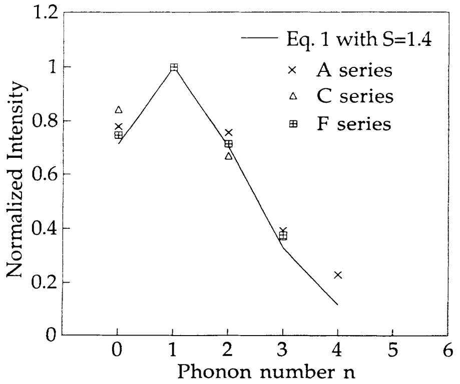

FIG. 3. The normalized intensities for the *A*, *C*, and *F* series are plotted versus phonon number *n*. A fitting procedure results in a mean value of the Huang-Rhys factor $S=1.4$, plotted as a full line, using Eq. (1).

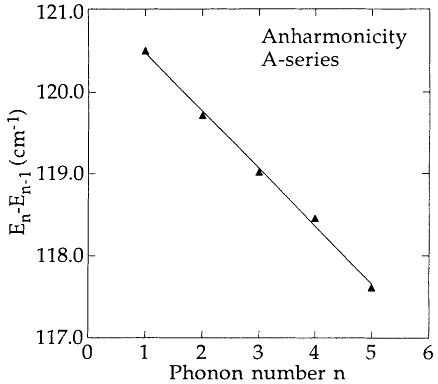

FIG. 4. Anharmonicity detected for the *A* series. (E_n-E_{n-1}) is plotted versus phonon number *n*. A linear fit results in a value of the phonon energy of 121.2 cm^{-1} and the anharmonicity constant $\sigma=2.8\times10^{-2}$.

The stress response of the *A*, *B*, *C*, and *D* series has been studied in some detail and in a first approximation they all show a similar splitting. The stress behavior of those sharper phonon replicas that were possible to study, showed a splitting identical to the zero-phonon lines, as is expected for replicas. The stress pattern of the C_0 line is presented in Fig. 5. Stress in the ⟨001⟩ direction results in a shift of the line but no splitting, whereas for stress in the ⟨110⟩ and ⟨111⟩ directions, the line splits into two components. This splitting pattern, i.e., the number of components for a given stress direction, is characteristic for transitions at trigonal centers between two nondegenerate electronic states. When the stress is applied in the ⟨001⟩ direction, all centers will be at the same angle to the stress direction and no splitting of the line is expected. In the case of stress in the ⟨111⟩ and ⟨110⟩ directions there are two nonequivalent orientations of the centers and the line should thus split into two components.

The data will be analyzed closely following Hughes and Runciman (*H*-*R*).[11] We consider a representative trigonal center with its threefold axis in the [111] direction. For small stress, the uniaxial stress operator, **V**, is expected to be accurately described by a linear response in the components of the stress tensor, σ. Reduction of the cubic representations into trigonal symmetry shows that the stress tensor contains two components of A_1 symmetry and two components of E symmetry. A_1 and E are irreducible representations of the C_{3v} point group of dimension one and two, respectively. We have here chosen to work with the notations of C_{3v}, although no distinction between the possible trigonal point groups can be made from uniaxial stress measurements. This choice does, however, not alter the evaluation of the stress and the polarization results. Since **V** must be invariant under the symmetry operations, the corresponding electronic operators transform identically to the stress tensor com-

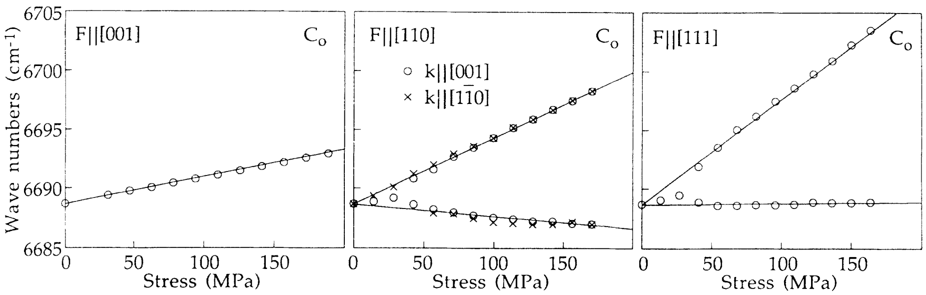

FIG. 5. The stress splitting of the C_0 line for $F\|[001]$, $F\|[110]$ with $k\|[001]$ and $k\|[1\bar{1}0]$, and for $F\|[111]$. The solid curves are the results from a fitting procedure with $\mathcal{A}_1=0.0232$ cm^{-1}/MPa and $\mathcal{A}_2=0.0332$ cm^{-1}/MPa.

ponents. The stress operator may then be written

$$\begin{aligned}\mathbf{V}=&\ \mathbf{A}_1(\sigma_{xx}+\sigma_{yy}+\sigma_{zz})+\mathbf{A}_1'(\sigma_{yz}+\sigma_{zx}+\sigma_{xy})\\ &+\mathbf{E}_\theta(2\sigma_{zz}-\sigma_{xx}-\sigma_{yy})+\sqrt{3}\mathbf{E}_\varepsilon(\sigma_{xx}-\sigma_{yy})\\ &+\mathbf{E}_\theta'(2\sigma_{xy}-\sigma_{yz}-\sigma_{zx})+\sqrt{3}\mathbf{E}_\varepsilon'(\sigma_{yz}-\sigma_{zx})\,, \end{aligned} \tag{3a}$$

where the tensor components σ_{ij} refer to the cubic axis. The electronic operators $\mathbf{A}_1$ and $\mathbf{A}_1'$ in Eq. 3(a) will only cause shifts of the level and thus describe the lifting of the orientational degeneracy whereas the two $\mathbf{E}$ operators lead to a splitting of an electronic state of E symmetry. In the case of an E state (basis E_θ and E_ε), the matrices of the electronic operators are defined as

$$\mathbf{E}_\theta=\mathbf{E}_\theta'=\begin{bmatrix}-1 & 0\\ 0 & 1\end{bmatrix},\quad \mathbf{E}_\varepsilon=\mathbf{E}_\varepsilon'=\begin{bmatrix}0 & 1\\ 1 & 0\end{bmatrix}\,. \tag{3b}$$

No thermalization effects were observed for the stress split components of any line which indicate that the initial state is nondegenerate and, therefore, has either A_1 or A_2 symmetry. The expected energy splittings of lines due to A-A and A-E transitions are summarized in Table IV where A collectively denotes a state of either A_1 or A_2 symmetry.

As established above, the splitting pattern of the C_0 line shown in Fig. 5 is typical for an A-A transition at a trigonal center. However, the same splitting pattern would also be observed for an A-E transition in which the splitting of the E state is too small to be detected. To obtain conclusive information of the symmetry of the final state, polarization experiments were carried out. The electron-dipole operator transforms as A_1+E in C_{3v} symmetry. The A_1 part corresponds to light polarized parallel to the trigonal axis, whereas the E part corresponds to light polarized perpendicular to the trigonal axis. A-A transitions are, therefore, of type π dipole while A-E transitions are of type σ dipole where we comply with the notation of Kaplyanskii.[12] The two types of electric-dipole transitions have unique polarization rules[11,12] which for clarity are presented in Table IV. It should be noted that, compared to the results by *H-R*, we have chosen the same normalization for the total intensity when $\mathbf{F}\|\langle 111\rangle$ as for the other directions. When stress was applied along the [110] axis, the propagation of incident light, $\mathbf{k}$, was either in the [001] or in the $[1\bar{1}0]$ direction. The electric vector of the light is labeled $\mathbf{E}$ in Table IV and the figures. The experimental results together with theoretical relative intensities are shown in Fig. 6. The good agreement between theory and experiment thus establish that the final state of the C series is of A symmetry (A_1 or A_2).

Since the C series involves transitions between nondegenerate electronic states, the two E operators in Eq. 3(a) may be excluded. Two parameters, $\mathcal{A}_1$ and $\mathcal{A}_2$, thus suffice to describe the stress splitting, where $\mathcal{A}_1$ and $\mathcal{A}_2$ are defined as the reduced matrix elements $\mathcal{A}_1$

TABLE IV. Energy shifts, intensity, and polarization rules for trigonal centers under uniaxial stress. The transitions are from a nondegenerate initial state of A (A_1 or A_2) symmetry to final states of A and E symmetry, following Refs. 11 and 12.

		A-A transitions			*A-E* transitions			
Stress direction	Energy shift	Intensities			Energy shift	Intensities		
		E‖**F**	**E**⊥**F**			**E**‖**F**	**E**⊥**F**	
F‖⟨001⟩	$\mathcal{A}_1$	4	4		$\mathcal{A}_1-2\mathcal{B}$	4	1	
					$\mathcal{A}_1+2\mathcal{B}$	0	3	
F‖⟨111⟩	$\mathcal{A}_1+2\mathcal{A}_2$	3	0		$\mathcal{A}_1+2\mathcal{A}_2$	0	$\frac{3}{2}$	
	$\mathcal{A}_1-(\frac{2}{3})\mathcal{A}_2$	1	4		$\mathcal{A}_1-(\frac{2}{3})\mathcal{A}_2-(\frac{4}{3})\mathcal{C}$	4	$\frac{1}{4}$	
					$\mathcal{A}_1-(\frac{2}{3})\mathcal{A}_2+(\frac{4}{3})\mathcal{C}$	0	$\frac{9}{4}$	
		E‖**F**	**E**⊥**F** **k**‖⟨001⟩	**E**⊥**F** **k**‖⟨110⟩		**E**‖**F**	**E**⊥**F** **k**‖⟨001⟩	**E**⊥**F** **k**‖⟨110⟩
F‖⟨110⟩	$\mathcal{A}_1+\mathcal{A}_2$	4	0	2	$\mathcal{A}_1+\mathcal{A}_2+\mathcal{C}-\mathcal{B}$	0	3	0
					$\mathcal{A}_1+\mathcal{A}_2-\mathcal{C}+\mathcal{B}$	1	0	2
	$\mathcal{A}_1-\mathcal{A}_2$	0	4	2	$\mathcal{A}_1-\mathcal{A}_2+\mathcal{C}+\mathcal{B}$	0	1	2
					$\mathcal{A}_1-\mathcal{A}_2-\mathcal{C}-\mathcal{B}$	3	0	0

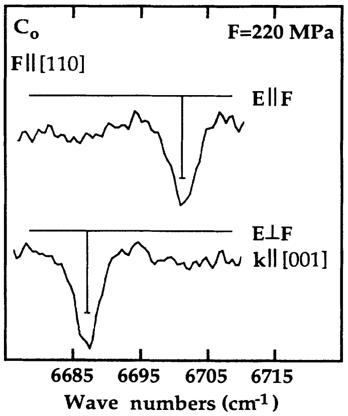

FIG. 6. Polarization spectra for the C_0 line for $F\|[110],k\|[001]$. The full lines are the theoretical relative intensities for an A-A transition of a trigonal center, listed in Table IV.

$=[\Gamma_f\|\mathbf{A}_1\|\Gamma_f]-[\Gamma_i\|\mathbf{A}_1\|\Gamma_i]$ and $\mathcal{A}_2=[\Gamma_f\|\mathbf{A}_1'\|\Gamma_f]-[\Gamma_i\|\mathbf{A}_1'\|\Gamma_i]$. Γ_i and Γ_f denote the initial and final state, respectively. A fitting to the experimental data was carried out and the full lines in Fig. 5 show the result for $\mathcal{A}_1=0.0232$ cm^{-1}/MPa and $\mathcal{A}_2=0.0332$ cm^{-1}/MPa. As seen, a good agreement with the experimental data was obtained.

A more complex stress splitting was observed for the A_0 line as depicted in Fig. 7(a). The new high-resolution experiments presented here fully resolve the stress-split components. With stress applied in the ⟨001⟩ direction, no splitting could be resolved whereas a small broadening of the line was detected which increases with increasing stress. This indicates that the line indeed splits but that the splitting is too small to be resolved. When the stress was applied in the ⟨111⟩ and ⟨110⟩ directions, the line splits into three and four components, respectively. This behavior is characteristic for an A-E transition of a trigonal center. Polarization experiments carried out for stress applied in the ⟨110⟩ and ⟨111⟩ directions confirm this assignment. This polarization spectra and, for a comparison, also the theoretical relative intensities are presented in Fig. 8(a) and 8(b). A good agreement between experiment and theory is obtained also for this line and we conclude that the A_0 line is due to an A-E transition.

According to H-R the stress splitting of the A_0 line may be described by four parameters labeled $\mathcal{A}_1$, $\mathcal{A}_2$, $\mathcal{B}$, and $\mathcal{C}$ (see Table IV). However, as is clearly seen in Fig. 7, the stress response of the A_0 line shows small but clear deviations from this linear model. There are no reasons to believe that the nonlinear response originates from the properties of the initial state since no such effects were observed for the C_0 line. We, therefore, have to consider a stress induced interaction between the A_0 final state of E symmetry and another state of a symmetry yet to be determined.

The splittings of the A_0 and C_0 lines show close similarities and, within the experimental uncertainty, the hydrostatic parameters $\mathcal{A}_1$ and $\mathcal{A}_2$ are identical for both the A_0 and C_0 lines. In Fig. 7(a), the dashed lines are obtained by using $\mathcal{B}=\mathcal{C}=0$ and the $\mathcal{A}_1$ and $\mathcal{A}_2$ values obtained from the C_0 line. As observed, the fitting lines closely follow the experimental points.

In our previous work on the Au-pair center,[8] the nonlinear response of the A_0 line was suggested to originate from a stress induced mixing between the final states of the A_0 and A_0' lines. To explain the stress splitting of the A_0 line it was concluded that the final state of the A_0' line must also have E symmetry. A good agreement with the experimental data was in this way obtained. Due to the low intensity of the A_0' line, its stress response could only be studied for F||⟨001⟩. The stress response in this direction for the A_0 and A_0' lines is the same. In this

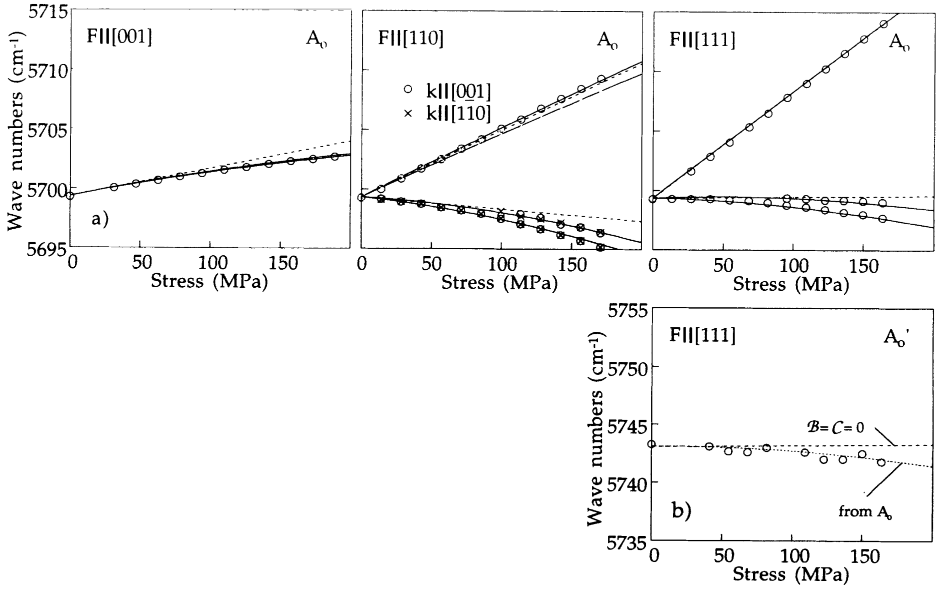

FIG. 7. (a) The stress splitting of the A_0 line for $F\|[001]$, $F\|[110]$ with $k\|[001]$ and $k\|[1\bar{1}0]$, and for $F\|[111]$. The solid curves are obtained from a fitting procedure which resulted in $\mathcal{A}_1=0.0232$ cm^{-1}/MPa, $\mathcal{A}_2=0.0332$ cm^{-1}/MPa, $\mathcal{B}=1.8\times10^{-4}$ cm^{-1}/MPa, $\mathcal{C}=2.7\times10^{-3}$ cm^{-1}/MPa, $\mathcal{A}_{1\mathrm{mix}}=-5.1\times10^{-2}$ cm^{-1}/MPa, and $\mathcal{A}_{2\mathrm{mix}}=2.3\times10^{-2}$ cm^{-1}/MPa. The dashed lines correspond to the case when $\mathcal{B}=\mathcal{C}=0$, (from the C_0 line in Fig. 5). (b) The stress splitting of the A_0' line for $F\|[111]$. The dotted line corresponds to the center of gravity of the two low-energy components of the A_0 line.

work, however, it was possible to partly study the A_0' line stress response for **F**$\|\langle 111\rangle$ depicted in Fig. 7(b). Only one A_0' component (or two unresolved components) could be studied but its energy shift agrees well with that for the center of gravity of the two lowest A_0 components. This behavior is incompatible with the previous assignment of a stress-induced mixing between the final states of the A_0 and A_0' lines. The A_0' line is, therefore, suggested to be a phonon replica of the A_0 line with a phonon energy of about $\hbar\omega' = 43.5$ cm^{-1}. The A_1' line could then be assigned to a two-phonon replica $\hbar\omega + \hbar\omega'$ above the A_0 line.

It is at this stage difficult to judge whether the A_0'' line is a zero-phonon line or a phonon replica of the A_0 line since no information of its stress behavior exists. In the latter case, it must involve a phonon of about $\hbar\omega'' = 92.3$ cm^{-1}. As is shown below there are strong additional reasons to believe that both the A' and A'' lines are phonon replicas. No other line series show phonon replicas involving $\hbar\omega'$ and $\hbar\omega''$ phonons which may indicate that our assignment is wrong. But since the A_0 line has high intensity and the smallest FWHM of all zero-phonon lines, whereas the A_0' and A_0'' lines have very low intensities, such phonon replicas for all other line series should be impossible to detect.

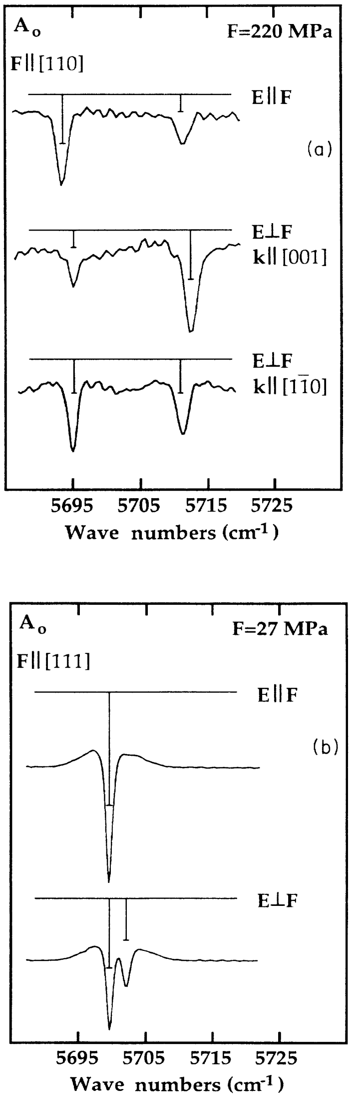

FIG. 8. Polarization spectra of the A_0 line for (a) $F\|[110]$ with $k\|[001]$ and $k\|[1\bar{1}0]$, and (b) $F\|[111]$. The vertical full lines are the theoretical relative intensities for an A-E transition of a trigonal center, listed in Table IV.

If the A_0'' line indeed is a zero-phonon line, its final state may very well be the E state which interacts with the A_0 line and causes its nonlinear stress behavior. In that case, the necessity for the A_0'' line final state to have E symmetry may be understood from the following discussion. By assuming that the final state of the A_0'' line has A symmetry, the mixing with the A_0 line E state must be governed by electronic operators of E symmetry since the direct product $E\otimes A$ equals E. Furthermore, when **F**$\|\langle 100\rangle$, Eq. 3(a) shows that only one of the E states (E_θ in the basis E_θ and E_ε) of the A_0 line will mix and, hence, only one of the two stress-split components will show a nonlinear stress response in contradiction with the experimental results. We are therefore forced to conclude that the final state of the A_0'' line also has E symmetry.

Twelve different stress parameters are generally needed to fully describe the stress response of the two E states of the A_0 and A_0'' lines. This is too many to allow for an analysis of their stress response and some assumptions and simplifications have to be made. The first assumption is that the values of the $\mathcal{A}_1$ and $\mathcal{A}_2$ parameters for the A_0'' line are identical to those of the A_0 and C_0 lines. In the second assumption, the $\mathcal{B}$ and $\mathcal{C}$ parameters (describing the lifting of the electronic degeneracy) are postulated to be the same for the two E states. This latter assumption is questionable since no information on the electronic splitting of the A_0'' line exists. However, the calculations show that the fitting to the experimental data for the A_0 line is to a high degree insensitive to the actual value of the $\mathcal{B}$ and $\mathcal{C}$ parameters of the A_0'' line. The number of parameters for first-order stress splitting of the two E states have thus been reduced from eight to four.

The interaction between the two E states is described by four parameters, $\mathcal{A}_{1\text{mix}}$, $\mathcal{A}_{2\text{mix}}$, $\mathcal{B}_{\text{mix}}$, and $\mathcal{C}_{\text{mix}}$ (as defined below). The total matrix describing both the splitting pattern and the interaction between the A and A'' series becomes

$$\begin{bmatrix} \alpha-\beta+E_{A_0} & \gamma & \alpha_{\text{mix}}-\beta_{\text{mix}} & \gamma_{\text{mix}} \\ \gamma & \alpha+\beta+E_{A_0} & \gamma_{\text{mix}} & \alpha_{\text{mix}}+\beta_{\text{mix}} \\ \alpha_{\text{mix}}-\beta_{\text{mix}} & \gamma_{\text{mix}} & \alpha-\beta+E_{A_0''} & \gamma \\ \gamma_{\text{mix}} & \alpha_{\text{mix}}+\beta_{\text{mix}} & \gamma & \alpha+\beta+E_{A_0''} \end{bmatrix}, \tag{4a}$$

where E_{A_0} and $E_{A_0''}$ are the energies of the zero-phonon lines in the A and A'' series, respectively, and

$$
\begin{aligned}
\alpha &= \mathcal{A}_1(\sigma_{xx}+\sigma_{yy}+\sigma_{zz})+2\mathcal{A}_2(\sigma_{yz}+\sigma_{zx}+\sigma_{xy})\ ,\\
\beta &= \mathcal{B}(2\sigma_{zz}-\sigma_{xx}-\sigma_{yy})+\mathcal{C}(2\sigma_{xy}-\sigma_{yz}-\sigma_{zx})\ ,\\
\gamma &= \sqrt{3}\mathcal{B}(\sigma_{xx}-\sigma_{yy})+\sqrt{3}\mathcal{C}(\sigma_{yz}-\sigma_{zx})\ ,\\
\alpha_{\text{mix}} &= \mathcal{A}_{1\text{mix}}(\sigma_{xx}+\sigma_{yy}+\sigma_{zz})\\
&\quad +2\mathcal{A}_{2\text{mix}}(\sigma_{yz}+\sigma_{zx}+\sigma_{xy})\ ,\\
\beta_{\text{mix}} &= \mathcal{B}_{\text{mix}}(2\sigma_{zz}-\sigma_{xx}-\sigma_{yy})\\
&\quad +\mathcal{C}_{\text{mix}}(2\sigma_{xy}-\sigma_{yz}-\sigma_{zx})\ ,\\
\gamma_{\text{mix}} &= \sqrt{3}\mathcal{B}_{\text{mix}}(\sigma_{xx}-\sigma_{yy})+\sqrt{3}\mathcal{C}_{\text{mix}}(\sigma_{yz}-\sigma_{zx})\ .
\end{aligned}
\tag{4b}
$$

The calculations showed that the mixing parameters $\mathcal{B}_{\text{mix}}$ and $\mathcal{C}_{\text{mix}}$ did not affect the splitting pattern of the A_0 line and, therefore, $\beta_{\text{mix}}=\gamma_{\text{mix}}=0$ in the calculations. This reduced the total number of mixing parameters to two, $\mathcal{A}_{1\text{mix}}$ and $\mathcal{A}_{2\text{mix}}$. The results from a fitting procedure are marked with full lines in Fig. 7(a) and the following parameters were obtained: $\mathcal{B}=1.8\times10^{-4}$ cm^{-1}/MPa, $\mathcal{C}=2.7\times10^{-3}$ cm^{-1}/MPa, $\mathcal{A}_{1\text{mix}}=-5.1\times10^{-2}$ cm^{-1}/MPa, and $\mathcal{A}_{2\text{mix}}=2.3\times10^{-2}$ cm^{-1}/MPa.

C. Zeeman experiments

The stress results presented above showed that the ground state has either A_1 or A_2 symmetry and, hence, could not split in an applied magnetic field. In trigonal symmetry, only states of E symmetry split in a Zeeman experiment and, therefore, the lines in the A series should split, whereas the C series remain unaffected. This was indeed also experimentally observed. No information of the Zeeman splitting of the other series could be obtained due to either their low intensity or their large FWHM compared to the expected splitting.

We attribute magnetic quantum numbers $m_J=\pm1$ to the two partners of the E final state of the A_0 line. The Zeeman energies for an E state at an axial center are then given by

$$E=m_J\mu_B B\sqrt{g_{\parallel}^2\cos^2\theta+g_{\perp}^2\sin^2\theta}\ , \tag{5}$$

where μ_B is the Bohr magneton. $g_{\parallel}$ and $g_{\perp}$ are the corresponding g values parallel and perpendicular to the axis of the center and θ is the angle between the C_3 axis of the center and the magnetic-field direction. In Fig. 9 the experimental data are shown for the A_0 line with $\mathbf{B}\|\langle 001\rangle$, $\langle 110\rangle$, and $\langle 111\rangle$. For $\mathbf{B}\|\langle 110\rangle$, two of the four possible directions of the centers are oriented perpendicular to the field direction. The central line that corresponds to these centers shows no splitting. This implies that $g_{\perp}\approx0$ and a fit to the data for all three field directions gives approximately $g_{\parallel}=1.1$. These results agree with the identification of the center to have trigonal symmetry since in that case $g_{\perp}\equiv0$. Finally, polarization experiments together with theoretical relative intensities are presented in Fig. 10(a) and 10(b) for $\mathbf{B}\|\langle 110\rangle$ and $\langle 111\rangle$. Theoretical energy shifts and polarization rules together with relative intensities are given in Table V for an A-E transition in trigonal symmetry. The good agreement between the results confirms the trigonal symmetry for the center.

D. Isothermal annealing

The activation energy for dissociation of the gold-pair center was determined by an isothermal annealing experiment. The annealing temperature was in the range 500–650 °C. By assuming that the dissociation of gold pairs during the annealing follows first-order reaction kinetics, the concentration $[\text{Au}_2]$ at time t is described by

$$[\text{Au}_2]=[\text{Au}_2]_0e^{-t/\tau} \tag{6}$$

where $[\text{Au}_2]_0$ is the initial concentration and t the annealing time. $1/\tau$ is the dissociation rate which is assumed to have a temperature dependence given by

$$\frac{1}{\tau}=\frac{1}{\tau_0}e^{-\Delta E/k_BT} \tag{7}$$

where ΔE is the activation energy for dissociation, k_B the Boltzmann constant, and T the annealing temperature. At constant temperature, the intensities of the A lines were measured after each of totally five 30 min anneals. Since the intensity is proportional to the gold-pair concentration, τ could be determined for each annealing temperature by using Eq. (6). In Fig. 11, the dissociation time constant, τ, is plotted versus annealing temperature, T. The experiments result in $\Delta E=1.7$ eV in acceptable agreement with the estimate by Ohta of 0.6–1.2 eV. This high dissociation energy indicates that the gold atoms occupy substitutional sites. In the case one or both gold atoms were in interstitial sites, a considerably lower value would be expected. The annealing study thus gives strong evidence for the center to consist of two substitutional gold atoms.

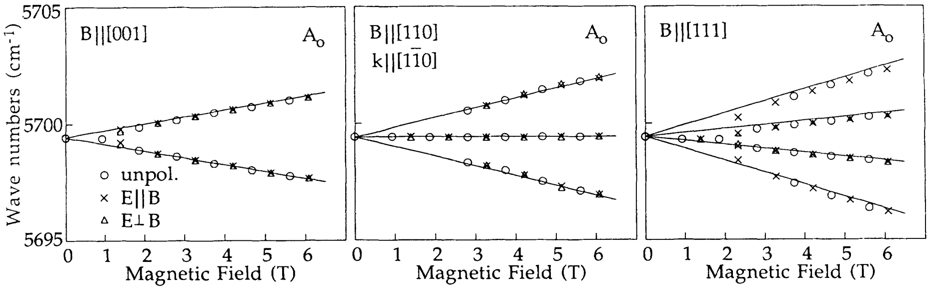

FIG. 9. Zeeman splitting of the A_0 line with $B\|[001]$, $B\|[110]$, and $B\|[111]$. Experimental data achieved from unpolarized light, $E\|B$, and $E\perp B$ are marked with ○, ×, and △, respectively. The solid curves are the results from a fitting procedure using Eq. (5) with $g_{\perp}=0$ and $g_{\parallel}=1.1$.

E. Model and final discussion

The electronic structure of substitutional Au in silicon has been suggested to be well accounted for by the "Watkins vacancy model.[13]" The vacancy one-electron states consist of an a_1 state in the valence band and a t_2 gap state and for the neutral vacancy, V^0, both orbitals are occupied by two electrons each, resulting in an $a_1^2t_2^2$ configuration. Neutral Au has the electron configuration $5d^{10}6s^1$ outside filled shells and according to the vacancy model, the filled $5d$ shell enters the valence band and the $6s$ electron is promoted to the t_2 vacancy orbital. The electronic structure of Au^0 should thus show close similarity with that for V^- concerning, e.g., Jahn-Teller distortions. Recently, strong support for such correspondence was presented.[3] Furthermore, calculations[1] have shown that substitutional Au in silicon indeed has a vacancylike electronic structure with a t_2 state in the band gap. Based on the experimental findings above, it is believed that the gold-related center studied in this paper is the substitutional gold-pair center with the Au atoms on nearest substitutional sites. Extrapolating the vacancy model for single substitutional gold to the gold-pair center it is assumed that its electronic structure could be described by a divacancy model, at least qualitatively. In a first approximation, the filled Au $5d$ shell, split by the trigonal crystal field, is expected to be inert and found as resonances in the valence band. The two gold atoms promote one $6s$ electron each to the neutral divacancy. In the following, the neutral gold-pair center will be discussed employing the electronic structure of the doubly negatively charged divacancy $V_2{}^{2-}$.

TABLE V. The Zeeman splitting, intensity, and polarization rules for an A-E transition at trigonal centers, ($\Delta = \mu_B B g_{\parallel}$).

Magnetic field direction	Energy shift	*A*-*E* Transitions		
		Intensities		
		E‖B	**E⊥B**	
B‖⟨001⟩	$+\Delta/\sqrt{3}$	8	8	
	$-\Delta/\sqrt{3}$	8	8	
B‖⟨111⟩	$+\Delta$	0	3	
	$+\Delta/3$	8	5	
	$-\Delta/3$	8	5	
	$-\Delta$	0	3	
		E‖B	**E⊥B** **k**‖⟨001⟩	**E⊥B** **k**‖⟨110⟩
B‖⟨110⟩	$+\Delta\sqrt{2/3}$	2	6	4
	± 0	12	4	8
	$-\Delta\sqrt{2/3}$	2	6	4

In the divacancy model, the undistorted $\mathrm{Au}_2{}^0$ ($V_2{}^{2-}$) center has trigonal D_{3d} symmetry and the lowest one-electron states are a_{1g}, a_{1u}, e_u, and e_g listed in order of increasing energy.[14] For the ground state, the one-particle states are successively filled by the 8 (6 from $V_2{}^0$ and 2 from the Au $6s$ states) available electrons assuming a low-spin configuration. The $\mathrm{Au}_2{}^0$ ground state should then have an $a_{1g}^2a_{1u}^2e_u^4$ configuration resulting in an ${}^1A_{1g}$

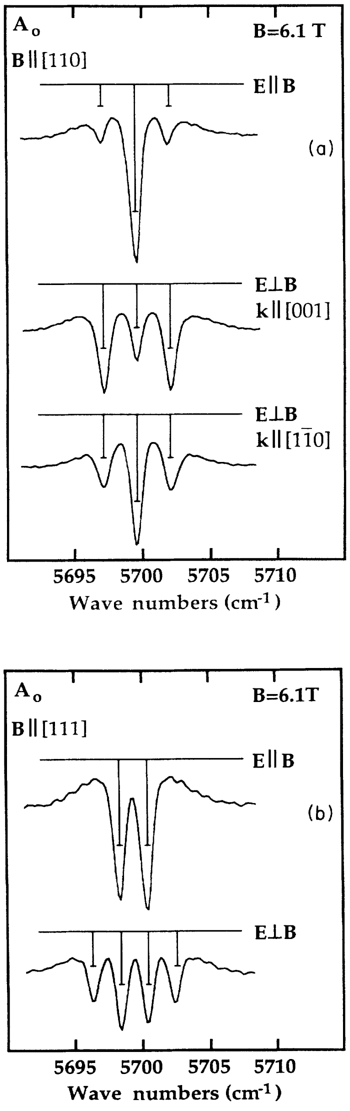

FIG. 10. Polarization spectra of the A_0 line for (a) $B\|[110]$ with $k\|[001]$ and $k\|[1\bar{1}0]$, and (b) $B\|[111]$. Calculated relative intensities for an A-E transition of a trigonal center are depicted as vertical full lines (see Table V).

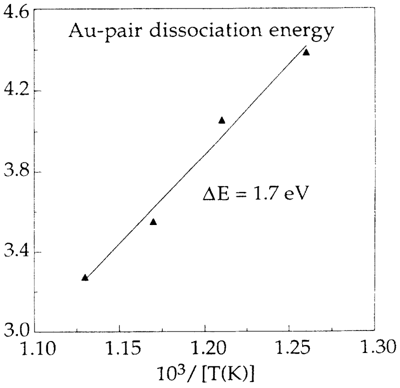

FIG. 11. Isothermal annealing results plotted as $\ln\tau$ versus $10^3/[T(\mathrm{K})]$. From the slope a dissociation energy of $\Delta E = 1.7$ eV is obtained.

(A_{1g}) ground-state term. So far, this model agrees with the experimental results from which it was established that the initial state of the transitions was an orbital singlet. The lowest excited states are expected when one of the e_u electrons is excited to the e_g state resulting in an $a_{1g}^2 a_{1u}^2 e_u^3 e_g^1$ configuration. The six terms in the *LS*-coupling scheme (i.e., *LS*-coupling, where L corresponds to the irreducible representations of D_{3d}) are ${}^{2S+1}A_{1u}$, ${}^{2S+1}A_{2u}$, and ${}^{2S+1}E_u$, where $S=0$ or 1. The accidental degeneracies are lifted by the *s-o* interaction which results in three levels of A_{1u} symmetry, three of A_{2u}, and five of E_u symmetry. In D_{3d}, the electric-dipole operator transforms as $A_{2u}+E_u$, and, therefore, only transitions to A_{2u} and E_u states are symmetry allowed from an A_{1g} initial state. Group theory thus predicts that transitions to eight different excited states are symmetry allowed. As is shown in the Appendix, only four of these are expected to be visible according to the divacancy model.

The final states in the transitions could be constructed by considering a hole in the e_u state coupled to an electron in the e_g state. The resulting energy-level structure is due to the *s-o* interaction and the direct and exchange Coulomb interaction between the two particles. The Coulomb interaction could be described by five parameters δ, Δ, γ, Γ, and ε defined in the Appendix. The relative magnitude of the parameters could not be calculated unless a more detailed model was employed which was beyond the scope of this investigation. The term energies relative to the common energy of $E_0+\delta$ are

$$\begin{aligned}
{}^1A_{1u}&:\ +\Delta+\gamma+\Gamma\\
{}^3A_{1u}&:\ -\Delta+\gamma-\Gamma\\
{}^1A_{2u}&:\ -\Delta-\gamma+\Gamma\\
{}^3A_{2u}&:\ +\Delta-\gamma-\Gamma\\
{}^1E_u&:\ +\varepsilon\\
{}^3E_u&:\ -\varepsilon\ ,
\end{aligned}\tag{8}$$

where E_0 is the sum of the one-particle energies for vanishing Coulomb interaction.

In D_{3d} symmetry, the *s-o* operator for an electron in the ${}^2e_g$ state has the form $H_{s\text{-}o}=\xi_g l_z s_z$, where z coincides with the trigonal axis. In the case of the hole in the ${}^2e_u$ state, $H_{s\text{-}o}=-\xi_u l_z s_z$. The complex basis $|\Gamma_{g,u}\mu\rangle=|e_{g,u}\pm1\rangle$ is employed and we define $\langle\Gamma_{g,u}\mu'|\xi_{g,u}l_z|\Gamma_{g,u}\mu\rangle\equiv\lambda_{g,u}\{\mathcal{L}_z\}_{\mu'\mu}$ and choose the matrix $\mathcal{L}_z\equiv2\mathrm{s}_z$. A one-to-one correspondence is in this way obtained between the row index μ and the m_l values for an e state derived from an atomic p orbital, i.e., a p isomorphism. l_z is the projection of the true angular momentum and s_z is the spin-$\frac{1}{2}$ matrix. The *s-o* interaction splits the ${}^2e_u$ and ${}^2e_g$ states into two spin doublets separated by $2\lambda_u$ and $2\lambda_g$, respectively. Four multiplets are then obtained by populating the spin-orbit levels (see Appendix). Their energy, relative to the center of gravity energy, becomes $E_1=+(\lambda_u+\lambda_g),[2E_u]$, $E_2=(\lambda_u-\lambda_g),[A_{1u}+A_{2u}+E_u]$, $E_3=-(\lambda_u-\lambda_g),[2A_{1u}+2A_{2u}]$, and $E_4=-(\lambda_u+\lambda_g),[2E_u]$, where the irreducible representations of the eigenstates (accidentally degenerate) in each set are listed in brackets.

The optical energies of the zero-phonon lines are structured into four well separated sets of nearby lines. The first set contains the A_0 line (excluding A_0'') which has an energy of 5699.4 cm^{-1}. The B_0, C_0, and D_0 lines form the second set centered at the mean value of 6675.0 cm^{-1} and the E_0 and F_0 lines constitute the last two sets at 7212.0 and 8147.1 cm^{-1}, respectively. Choosing the origin of energy at the first set, the sets appear at $E=0$, 975.6, 1512.6, and 2447.7 cm^{-1}.

In a first attempt to explain the observed energies for the sets, it is assumed that the *s-o* interaction exceeds that for the Coulomb interactions. This is a reasonable starting point since the heavy element Au is involved in the center. The one-particle orbitals e_u and e_g are linear combinations of divacancy orbitals (p like) and Au d orbitals, and according to the divacancy model, the amount of p character exceeds the d part. An atomic d state splits in a cubic crystal field into an e (labeled de_1) and a t_2 state separated by the energy Δ_{cubic}. Superimposing a trigonal crystal field, the t_2 state splits further into an a_1 and an e state (denoted de_2). When the strength of the trigonal field is much less than the cubic field, i.e., no mixing of the two de states, the matrix elements of l_z is zero for de_1 and ±1 for de_2. However, when the trigonal crystal field is much stronger than the cubic field, the projection of the true angular momentum, m_l, on the trigonal axis becomes a good quantum number and $m_l=\pm1$ and $m_l=\pm2$ for the two de states. As described above we generally denote an e state $|\Gamma\mu\rangle$ using a p isomorphism. It could be shown that the $|de\pm1\rangle$ states transform equally as the $|pe\pm1\rangle$ states, (i.e., e states derived from an atomic p state), whereas, e.g., the $|de+2\rangle$ transforms as an $|pe-1\rangle$ state under rotations in the trigonal point group. Hence, the e_g state of the gold-pair center then generally could be written as $|e_g\pm1\rangle=\alpha_g|pe_g\pm1\rangle+\beta_g|de_g\pm1\rangle+\gamma_g|de_g\mp2\rangle$, where $|\alpha_g|^2+|\beta_g|^2+|\gamma_g|^2=1$, and similarly for the e_u state. The matrix elements of $\xi_g l_z$ among the $|e_g\pm1\rangle$ states equal $\{\xi^p|\alpha_g|^2+\xi^d(|\beta_g|^2-2|\gamma_g|^2)\}\mathcal{L}_z$. The *s-o* parameters $\lambda_{g,u}$ are then determined by $\{\xi^p|\alpha_{g,u}|^2+\xi^d(|\beta_{g,u}|^2-2|\gamma_{g,u}|^2)\}$. The size and sign of λ_g and λ_u do not only depend on the relative amount of p and d character, but also on which type of d character that dominates, i.e., the relative amount of $|de\pm2\rangle$ and $|de\pm1\rangle$ states in the wave functions. In a first approximation, the divacancy model predicts that the wave functions of the e states in the band gap are mainly built up by the divacancy orbitals, i.e., they are p like. However, it is expected that the *s-o* interaction is governed by the d-like part since for atomic Au, ξ exceeds by far that for the Si dangling-bond orbitals. Assuming that for both the e_u and e_g states the inclusion in the wave function of $|de\pm1\rangle$ and $|de\pm2\rangle$ states are about equal, the *s-o* parameters λ_u and λ_g both become negative. When λ_u and λ_g have the same sign the lowest energy state corresponds to two accidentally degenerate E_u states as was shown above. We assume that both λ_u and λ_g are negative, which seems to be the most reasonable choice. The lowest energy state is then found at an energy E_1 as defined above. By defining an origin of the energy at E_1 and assuming that $|\lambda_u|>|\lambda_g|$, the different energy states are found at the energies 0, $-2\lambda_g$, $-2\lambda_u$, and $-2(\lambda_u+\lambda_g)$, for E_1, E_2, E_3, and E_4, respectively. This model predicts the energy of the two intermediate sets to add up to the energy of the upper set. The experimentally obtained energies give $975.6+1512.6\ \text{cm}^{-1}=2488.2\ \text{cm}^{-1}$, which indeed is close to the energy of $2447.7\ \text{cm}^{-1}$ obtained for the F_0 line. Both *s-o* parameters could thus be estimated and $\lambda_g\approx-488\ \text{cm}^{-1}$ and $\lambda_u\approx-756\ \text{cm}^{-1}$ were obtained. Disregarding the signs, these values are much larger than expected for the divacancy *p*-like orbitals, which indicate that the inclusion of *d* character indeed is substantial. The values estimated for the one-particle *s-o* parameter ξ^d for free 5*d* ions are in the range of 2000–3000 cm^{-1} (Ref. 15) and we use $\xi^d\approx2500\ \text{cm}^{-1}$ for the gold-pair center. Since $\xi^p\ll\xi^d$, $\lambda_{g,u}$ could be approximated by $\xi^d(|\beta_{g,u}|^2-2|\gamma_{g,u}|^2)$. The amount of *d* character could not be determined but the divacancy model is expected to be valid when the inclusion of *d* character is much less than the amount of *p* character. We therefore assume that the divacancy model could be applicable to describe the gold-pair center when the amount of *d* character is 25% or less. The minimum amount of *d* character in the wave functions is obtained when $|\beta_{g,u}|=0$ leading to $|\gamma_{g,u}|^2=\lambda_{g,u}/(2\xi^d)$ which gives approximately 10% and 15% *d* character for e_g and e_u, respectively. When $|\beta_{g,u}|=|\gamma_{g,u}|$, the e_g and e_u states have 40% and 60% *d* character, respectively, which by far exceeds the 25% that are consistent with a divacancy model. We may therefore conclude that the experimentally determined values for the *s-o* parameters are consistent with the divacancy model when $|\beta_{g,u}|<|\gamma_{g,u}|$.

According to the divacancy model, only four lines should be visible with final states, $E_u^a(E_1)$, $E_u^a(E_4)$, $A_{2u}(E_2)$, and $A_{2u}^a(E_3)$ (see Appendix). An identification of the corresponding experimental lines could be obtained by assuming that those four lines that have a considerably higher relative intensity correspond to the symmetry and divacancy allowed transitions to these four final states. In this way, the following identification was obtained: $A_0\leftrightarrow E_u^a(E_1)$, $C_0\leftrightarrow A_{2u}(E_2)$, $E_0\leftrightarrow A_{2u}^a(E_3)$, and $F_0\leftrightarrow E_u^a(E_4)$.

The energy positions of the B_0 and D_0 lines are close to that for the C_0 line. In a first approximation, we assume that the Coulomb interaction only splits the states in each *s-o* manifold and exclude any crossing of the *s-o* levels. It is therefore reasonable to assume that the B_0 and D_0 final states originate from the *s-o* manifold of states at E_2, $E_u(E_2)$, and $A_{1u}(E_2)$. However, transitions to an A_{1u} state is strictly forbidden and could only become visible when the symmetry departs from being trigonal. The results from the stress and Zeeman experiments were all well accounted for by assuming trigonal symmetry. However, a small distortion of the Au atoms from their positions on the C_3 axis could remain undetected in the perturbation experiments.

To explain the observation of transitions to an A_{1u} state, effects beyond our simple model has to be taken into account. It is not surprising that we observe symmetry-allowed transitions although they are not allowed according to our divacancy model. There are always higher-order terms in the exact Hamiltonian that will mix states of the same symmetry. However, as was pointed out above, the observation of lines that are forbidden by group theory must be caused by a distortion that changes the point-group symmetry from trigonal to a lower one. A first possibility is that the center has a third component of yet unknown identity at an off-axis position which slightly disturbs the electronic structure of the gold-pair center from that given by the divacancy model.

A second possibility is a coupling between the electronic and vibrational subsystems, i.e., a Jahn-Teller effect (JT). A trigonal D_{3d} center has four different vibrational modes with symmetry A_{1g}, A_{2u}, E_g, and E_u. The electron-phonon coupling responsible for the pronounced phonon replicas observed in the spectrum was assumed to be one dimensional, i.e., either of A_{1g} or A_{2u} symmetry. To lowest order, the electron-phonon coupling $\mathbf{H}_{e\text{-ph}}$ is described by

$$\mathbf{H}_{e\text{-ph}}=\sum_{\Gamma_\mu}V_\Gamma\mathbf{U}_{\Gamma\mu}Q_{\Gamma\mu}\ , \tag{9}$$

where V_Γ is the strength of the interaction, $\mathbf{U}_{\Gamma\mu}$ is an electronic operator and $Q_{\Gamma\mu}$ is the distortion associated to the phonon mode belonging to the irreducible representation Γ and row index μ (see Appendix). Since the electronic final states are ungerade only the gerade modes are active in the electron-phonon coupling within this manifold of many-particle states. The ungerade modes, however, could cause an interaction between the e_g and e_u one-particle states and, hence, result in that parity fails to be a good quantum number. Such a mixing of the one-particle states is, however, expected to be weak since the energy separation between the e_g and e_u states is of the order of 800 meV. We therefore only consider the gerade modes in the following discussion. An A_{1g} or E_g distortion preserve the inversion symmetry and *u* and *g* remain to be good quantum numbers. In a first approximation, the gold atoms are assumed to vibrate whereas the Si neighbors are rigid at their equilibrium positions. The A_{1g} mode corresponds to a movement of the gold atoms 180° out of phase along the trigonal axis and in the E_g modes, the gold atoms move 180° out of phase in two perpendicular directions which both are perpendicular to the C_3 axis.

A coupling to the A_{1g} mode only shifts the energy of the electronic states. We are searching for an effect that transfers dipole strength from the allowed transitions to the unperturbed states of A_{1u} symmetry and which must involve a lowering of the electronic symmetry. A coupling to the E_g modes leading to a JT effect in the static regime will mix the final states of the intense A_{2u} and E_u lines with two of the A_{1u} final states. As is shown in the Appendix, there is no first-order coupling in the E_u states, whereas there are off-diagonal matrix elements coupling the various E_u, A_{2u}, and A_{1u} states, i.e., a pseudo Jahn-Teller effect. It is beyond the scope of this paper to solve the JT matrix for the adiabatic potentials. However, inspection of the JT matrix shows that within the divacancy model, altogether six lines could become visible of which four are intense and two are weak (the two A_{1u} lines).

This result gives additional proof for our interpretation of the weak A_0' and A_0'' lines as being phonon replicas of the A_0 line. When excluding these two lines as zero-phonon lines altogether six lines are indeed experimentally observed of which four have considerably higher intensity (A_0, C_0, E_0, and F_0) compared to that for the other two lines (B_0 and D_0) in full agreement with the divacancy model and a static JT effect. However, this analysis shows that the assumption that the B_0 and D_0 originate from the *s-o* manifold at E_2 fails, since in that case, the B_0 and D_0 final states must be associated with $E_u(E_2)$ and $A_{1u}(E_2)$. The JT analysis shows that the two states that could gain intensity by a static JT distortion originate from the E_2 and E_3 *s-o* manifolds, i.e., $A_{1u}(E_2)$ and $A_{1u}^a(E_3)$. This could indicate that, although our values of the *s-o* parameters satisfactory predict the relative energies of the sets of lines, the *s-o* parameters have about the same amplitude and/or the Coulomb interaction is somewhat stronger than assumed above.

The phonon mode responsible for the sharp phonon replicas in the spectrum remains to be identified. It is interesting to note that the phonon energy for the $\mathrm{Au_2}^0$ center exceeds that for the $\mathrm{Au_2}^-$ center. This could easily be explained within the divacancy model. In the $\mathrm{Au_2}^0$ final states, three electrons occupy a bonding orbital and the fourth occupies an antibonding orbital, whereas for $\mathrm{Au_2}^-$ three electrons occupy a bonding orbital and two an antibonding orbital. It is thus expected that the force constant is higher for the $\mathrm{Au_2}^0$ center compared to that for the $\mathrm{Au_2}^-$ center, i.e., that a mode softening should be observed when going from $\mathrm{Au_2}^0$ to $\mathrm{Au_2}^-$. Also, in this case, we believe that it is reasonable to only consider the gerade modes for similar reasons as discussed above. The A_{1g} is a symmetric stretching mode, whereas the E_g mode is a transverse (wagging) mode with respect to the C_3 axis. A considerable more pronounced mode softening is thus expected for the A_{1g} than for the E_g mode. Since, for given charge state, all line series show the same phonon energy and Huang-Rhys factor, the same mode is active in all series. Furthermore, the electron-phonon coupling in the electronic final states is described by matrix elements of type $\langle \Gamma_i | Q | \Gamma_i \rangle$, where Q is the configuration coordinate and Γ_i represents the electronic state under consideration. Since $\Gamma_i = A_{1u}$, A_{2u}, or E_u, and $A_{2u} \otimes A_{2u} = A_{1g}$, all different matrix elements are nonzero only when Q transforms as A_{1g}.

The phonon replicas, thus, originate from an electron-phonon coupling involving the A_{1g} mode, whereas the JT effect involves the E_g mode. It is difficult to conclusively identify the symmetry of the $\hbar\omega' = 43.5$ cm^{-1} and the $\hbar\omega'' = 92.3$ cm^{-1} modes. However, at least one of these must be associated with the ungerade modes whereas the other may very well be associated with the E_g JT mode.

Since it is now established that the A' and A'' lines are phonon replicas to the A_0 line an explanation to the nonlinear stress behavior detected for the A_0 line is needed. The only possibility that remains to investigate which also is compatible with the divacancy model is that the $E_u^a(E_1)$ state mixes with the other zero-phonon states. Considering the large energy distance, ≈ 1000 cm^{-1} between the A_0 and the B_0, C_0, and D_0 lines and even larger for the E_0 and F_0 lines, such stress induced mixing seems at a first glance unlikely. However, we have solved the full stress Hamiltonian in the basis of the $E_u^a(E_1)$, $A_{1u}(E_2)$, $A_{2u}(E_2)$, $A_{1u}^a(E_3)$, $A_{2u}^a(E_3)$, and $E_u^a(E_4)$ states and obtained an almost perfect fit for both the A_0 and C_0 lines which was identical to the results presented in Figs. 5 and 7. The best fit was obtained with $E_g = 0.071$ cm^{-1}/MPa, $E_g' = -0.1312$ cm^{-1}/MPa, $E_u = 0.361$ cm^{-1}/MPa, and $E_u' = 0.028$ cm^{-1}/MPa and the parameters and the full stress matrix are defined in the Appendix.

IV. CONCLUSIONS

Fourier-transform infrared spectroscopy on gold-doped silicon using both uniaxial stress and magnetic field have been performed. Thirteen different characteristic line series have been identified of which 11 consist of a relatively intense zero-phonon line followed by several phonon replicas. These series are assumed to be due to internal transitions at the same gold center in two different charge states which is supported by doping experiments. Annealing experiments indicate that the center consists of two nearest-neighbor substitutional gold atoms because of the high dissociation energy of $\Delta E = 1.7$ eV. Stress and Zeeman measurements show that the symmetry of the center is trigonal. It was possible to determine the symmetry of the final states of the A and C series to be of E and A symmetry, respectively, by using polarized light.

A divacancy model has been employed which successfully gives a qualitative understanding of the electronic structure of the gold-pair center. It has been assumed that the *s-o* interaction is much stronger than the electron-electron interaction and the two *s-o* parameters λ_u and λ_g were estimated to be about -760 and -490 cm^{-1}, respectively. The considerable variation in the relative intensity of the lines, four intense (E_u and A_{2u} final state symmetry) and two less intense lines (A_{1u} final state symmetry), was fully explained by the model. A Jahn-Teller effect in the static regime was suggested to slightly lower the symmetry from D_{3d} to a lower symmetry and transfer dipole strength to the two "symmetry forbidden" A_{1u} lines.

APPENDIX

The initial and final states are constructed as linear combinations of Slater determinants involving the four bound electrons. In the excited states three electrons occupy the ${}^2e_u$ state but it is more convenient to consider a hole in the ${}^2e_u$ state instead. In calculating the relative intensities below, a standard order must be chosen for the orbitals in the Slater determinants. The one-particle electron and hole states are denoted $|m_j\rangle_g$ and $|m_j\rangle_u$, respectively, where $m_j=m_l+m_s$ and $m_l=\pm 1$ and $m_s=\pm\frac{1}{2}$. In D_{3d} symmetry, the first-order *s-o* interaction for an electron in the ^2e_g state is diagonal in this basis and has the eigenvalues $\lambda_g|m_j|$ and for the hole in ^2e_u, the eigenvalues are $-\lambda_u|m_j|$. When populating the one-particle states in the 16 possible ways, the energy relative to the center of gravity becomes

$$E_1=(\lambda_u+\lambda_g),[\,|\pm 1/2\rangle_u|\pm 3/2\rangle_g\,]\ ,$$

$$E_2=(\lambda_u-\lambda_g),[\,|\pm 1/2\rangle_u|\pm 1/2\rangle_g\,]\ ,$$

$$E_3=-(\lambda_u-\lambda_g),[\,|\pm 3/2\rangle_u|\pm 3/2\rangle_g\,]\ ,$$

and

$$E_4=-(\lambda_u+\lambda_g),[\,|\pm 3/2\rangle_u|\pm 1/2\rangle_g\,]\ ,$$

where the populated one-particle product states are listed in brackets. All eigenstates are fourfold accidentally degenerate.

Using the coupling coefficients in Ref. 16, the irreducible representations can be found in terms of linear combination of the basis functions.

E_1:

$$\begin{aligned}
\psi_1(E_1^a)&=|-\tfrac{1}{2}\rangle_u|-\tfrac{3}{2}\rangle_g\ ,\\
\psi_1(E_{-1}^a)&=-|\tfrac{1}{2}\rangle_u|\tfrac{3}{2}\rangle_g\ ,\\
\psi_1(E_1^b)&=|-\tfrac{1}{2}\rangle_u|\tfrac{3}{2}\rangle_g\ ,\\
\psi_1(E_{-1}^b)&=|\tfrac{1}{2}\rangle_u|-\tfrac{3}{2}\rangle_g\ ,
\end{aligned}\tag{A1a}$$

E_2:

$$\begin{aligned}
\psi_2(A_1)&=\frac{|-\frac{1}{2}\rangle_u|\frac{1}{2}\rangle_g-|\frac{1}{2}\rangle_u|-\frac{1}{2}\rangle_g}{\sqrt{2}}\ ,\\
\psi_2(A_2)&=i\frac{|-\frac{1}{2}\rangle_u|\frac{1}{2}\rangle_g+|\frac{1}{2}\rangle_u|-\frac{1}{2}\rangle_g}{\sqrt{2}}\ ,\\
\psi_2(E_1)&=|\tfrac{1}{2}\rangle_u|\tfrac{1}{2}\rangle_g\ ,\\
\psi_2(E_{-1})&=|-\tfrac{1}{2}\rangle_u|-\tfrac{1}{2}\rangle_g\ ,
\end{aligned}\tag{A1b}$$

E_3:

$$\begin{aligned}
\psi_3(A_1^a)&=\frac{|\frac{3}{2}\rangle_u|-\frac{3}{2}\rangle_g-|-\frac{3}{2}\rangle_u|\frac{3}{2}\rangle_g}{\sqrt{2}}\ ,\\
\psi_3(A_1^b)&=-\frac{|\frac{3}{2}\rangle_u|\frac{3}{2}\rangle_g+|-\frac{3}{2}\rangle_u|-\frac{3}{2}\rangle_g}{\sqrt{2}}\ ,\\
\psi_3(A_2^a)&=-i\frac{|\frac{3}{2}\rangle_u|-\frac{3}{2}\rangle_g+|-\frac{3}{2}\rangle_u|\frac{3}{2}\rangle_g}{\sqrt{2}}\ ,\\
\psi_3(A_2^b)&=-i\frac{|\frac{3}{2}\rangle_u|\frac{3}{2}\rangle_g-|-\frac{3}{2}\rangle_u|-\frac{3}{2}\rangle_g}{\sqrt{2}}\ ,
\end{aligned}\tag{A1c}$$

E_4:

$$\begin{aligned}
\psi_4(E_1^a)&=|-\tfrac{3}{2}\rangle_u|-\tfrac{1}{2}\rangle_g\ ,\\
\psi_4(E_{-1}^a)&=-|\tfrac{3}{2}\rangle_u|\tfrac{1}{2}\rangle_g\ ,\\
\psi_4(E_1^b)&=|\tfrac{3}{2}\rangle_u|-\tfrac{1}{2}\rangle_g\ ,\\
\psi_4(E_{-1}^b)&=|-\tfrac{3}{2}\rangle_u|\tfrac{1}{2}\rangle_g\ .
\end{aligned}\tag{A1d}$$

The exact form of the Coulomb potential, $V(\mathbf{r}_1,\mathbf{r}_2)$, between the two particles is not known *a priori* but in D_{3d} symmetry it must transform as A_{1g} and is symmetric under a permutation of the indices $V(\mathbf{r}_1,\mathbf{r}_2)=V(\mathbf{r}_2,\mathbf{r}_1)$. The number of independent parameters needed to fully describe the Coulomb interaction is as much as five which may be understood by the following. The matrix elements are of type

$$\int\int a^*(\mathbf{r}_1)b^*(\mathbf{r}_2)V(\mathbf{r}_1,\mathbf{r}_2)c(\mathbf{r}_1)d(\mathbf{r}_2)d\mathbf{r}_1d\mathbf{r}_2\ ,\tag{A2}$$

where a, b, c, and d are orbitals of e_u (basis functions u_1 and u_{-1}) and of e_g (basis functions v_1 and v_{-1}). When both a and c belong to e_u (b and d belong to e_g), the product functions $a^*(\mathbf{r}_1)c(\mathbf{r}_1)$ are reducible into the irreducible representations $A_{1g}(\mathbf{r}_1)$ and $E_g^{\pm 1}(\mathbf{r}_1)$, [$\pm 1$ denotes the row index and only symmetrized products are nonzero which excludes $A_{2g}(\mathbf{r}_1)$ in the direct product], and similarly for b and d [$A_{1g}(\mathbf{r}_2)$ and $E_g^{\pm 1}(\mathbf{r}_2)$]. Since $V(\mathbf{r}_1,\mathbf{r}_2)$ transforms as A_{1g}, only three matrix elements are nonzero: $\int\int A_{1g}(\mathbf{r}_1)V(\mathbf{r}_1,\mathbf{r}_2)A_{1g}(\mathbf{r}_2)d\mathbf{r}_1d\mathbf{r}_2$ and $\int\int E_g^m(\mathbf{r}_1)V(\mathbf{r}_1,\mathbf{r}_2)E_g^{-m}(\mathbf{r}_2)d\mathbf{r}_1d\mathbf{r}_2$ with ($m=\pm 1$), denoted symbolically. However, the two last matrix elements are equal by the Wigner-Eckhardt theorem. Using similar arguments, three independent parameters are needed when a belongs to e_u and c belongs to e_g (or vice versa) and linear combinations of their products could be constructed transforming as $A_{1g}(\mathbf{r}_1)$, $A_{2g}(\mathbf{r}_1)$, and $E_g^{\pm 1}(\mathbf{r}_1)$ and similarly for b and d. The electron-electron interaction thus splits the 16-fold degenerate $a_{1g}^2a_{1u}^2e_u^3e_g^1$ configuration into six terms: $^{2S+1}A_{1u}$, $^{2S+1}A_{2u}$, and $^{2S+1}E_u$, where $S=0$ or 1. The various matrix elements are calculated in the $|S\Gamma M_s\mu\rangle$ basis in which the electron-electron interaction is diagonal. The five independent parameters are defined by

$$\begin{aligned}
\delta&=\int\int u_1^*(\mathbf{r}_1)v_1^*(\mathbf{r}_2)V(\mathbf{r}_1,\mathbf{r}_2)u_1(\mathbf{r}_1)v_1(\mathbf{r}_2)d\mathbf{r}_1d\mathbf{r}_2\ ,\\
\Delta&=\int\int u_{-1}^*(\mathbf{r}_1)v_1^*(\mathbf{r}_2)V(\mathbf{r}_1,\mathbf{r}_2)v_{-1}(\mathbf{r}_1)u_1(\mathbf{r}_2)d\mathbf{r}_1d\mathbf{r}_2\ ,\\
\gamma&=\int\int u_{-1}^*(\mathbf{r}_1)v_1^*(\mathbf{r}_2)V(\mathbf{r}_1,\mathbf{r}_2)u_1(\mathbf{r}_1)v_{-1}(\mathbf{r}_2)d\mathbf{r}_1d\mathbf{r}_2\ ,\\
\Gamma&=\int\int u_{-1}^*(\mathbf{r}_1)v_1^*(\mathbf{r}_2)V(\mathbf{r}_1,\mathbf{r}_2)v_1(\mathbf{r}_1)u_{-1}(\mathbf{r}_2)d\mathbf{r}_1d\mathbf{r}_2\ ,\\
\varepsilon&=\int\int u_{-1}^*(\mathbf{r}_1)v_{-1}^*(\mathbf{r}_2)V(\mathbf{r}_1,\mathbf{r}_2)v_{-1}(\mathbf{r}_1)u_{-1}(\mathbf{r}_2)d\mathbf{r}_1d\mathbf{r}_2\ .
\end{aligned}\tag{A3}$$

The full 16×16 Hamiltonian including both the electron-electron and *s-o* interaction could be factorized into smaller matrices.

The five states of E_u symmetry

$$\begin{array}{cc|l} \psi_1(E^a_{\pm1}) & \psi_4(E^a_{\pm1}) & \\ \delta+\dfrac{\lambda_u+3\lambda_g}{2} & -\varepsilon & \psi_1(E^a_{\pm1}) \\ -\varepsilon & \delta-\dfrac{3\lambda_u+\lambda_g}{2} & \psi_4(E^a_{\pm1}) \end{array} , \qquad \text{(A4a)}$$

$$\begin{array}{cc|l} \psi_1(E^b_{\pm1}) & \psi_4(E^b_{\pm1}) & \\ \delta-\Gamma+\dfrac{\lambda_u+3\lambda_g}{2} & -\Delta+\gamma & \psi_1(E^b_{\pm1}) \\ -\Delta+\gamma & \delta-\Gamma-\dfrac{3\lambda_u+\lambda_g}{2} & \psi_4(E^b_{\pm1}) \end{array} , \qquad \text{(A4b)}$$

$$E(\psi_2(E_{\pm1}))=\delta-\varepsilon+\frac{\lambda_u-\lambda_g}{2} . \qquad \text{(A4c)}$$

The three A_{1u} states:

$$\begin{array}{cc|l} \psi_2(A_1) & \psi_3(A^a_1) & \\ \delta+\Delta+\dfrac{(\lambda_u-\lambda_g)}{2} & \gamma+\Gamma & \psi_2(A_1) \\ \gamma+\Gamma & \delta+\Delta-\dfrac{3(\lambda_u-\lambda_g)}{2} & \psi_3(A^a_1) \end{array} , \qquad \text{(A4d)}$$

$$E(\psi_3(A^b_1))=\delta-\varepsilon-\frac{3(\lambda_u-\lambda_g)}{2} . \qquad \text{(A4e)}$$

The three A_{2u} states:

$$\begin{array}{cc|l} \psi_2(A_2) & \psi_3(A^a_2) & \\ \delta-\Delta+\dfrac{(\lambda_u-\lambda_g)}{2} & -\gamma+\Gamma & \psi_2(A_2) \\ -\gamma+\Gamma & \delta-\Delta-\dfrac{3(\lambda_u-\lambda_g)}{2} & \psi_3(A^a_2) \end{array} , \qquad \text{(A4f)}$$

$$E(\Psi_3(A^b_2))=\delta-\varepsilon-\frac{3(\lambda_u-\lambda_g)}{2} . \qquad \text{(A4g)}$$

Electric-dipole transitions

The electric-dipole operator could be written $\mathbf{D}_0=e_0r_0-(e_1r_{-1}+e_{-1}r_1)$ where $r_0=z$, $r_\pm=\mp(x\pm iy)/\sqrt{2}$ and the spherical components of the polarization vector are $e_0=e_z$, $e_\pm=\mp(e_x\pm ie_y)/\sqrt{2}$. The $\mathbf{D}_0$ matrix describing the electron transitions from the e_u states to the e_g states is written

$$\mathbf{D}_0=\begin{array}{cc|l} e_{u-1} & e_{u1} & \\ ie_0A & e_{-1}E & e_{g-1} , \\ e_1E & -ie_0A & e_{g1} \end{array} \qquad \text{(A5)}$$

where the parameters A and E are defined by $A=\langle e_{g-1}|r_0|e_{u-1}\rangle$ and $E=\langle e_{g1}|r_1|e_{u-1}\rangle$. By using the values of the elements in $\mathbf{D}_0$ the intensities are calculated for the symmetry allowed transitions from the A_{1g} ground state to the various excited states. The intensities are found in Table VI where common factors in the intensity are excluded. According to this table only four lines should be possible to detect. Furthermore, our definition of, e.g., the E^a and E^b states at E_1 above ensures that no mixing by the electron-electron interaction could transfer dipole strength from allowed to unallowed transitions.

The Jahn-Teller matrix and the full stress matrix

The interaction between the electronic states due to the coupling to the E_g distortions is explicitly described by

$$\mathbf{H}_{\mathrm{JT}}=V_g\frac{(\mathbf{U}^+Q^-+\mathbf{U}^-Q^+)}{\sqrt{2}}+V_u\frac{(\mathbf{V}^+Q^-+\mathbf{V}^-Q^+)}{\sqrt{2}} , \qquad \text{(A6)}$$

where V_g and V_u are the coupling coefficients for the e_u and e_g states, respectively. The electronic operators $\mathbf{U}^\pm$ and $\mathbf{V}^\pm$ only operate on the e_u and e_g states, respectively. $\mathbf{U}^\pm$ and $\mathbf{V}^\pm$ are defined by

$$\mathbf{U}^+=\mathbf{V}^+=\begin{bmatrix} 0 & 1 \\ 0 & 0 \end{bmatrix} , \qquad \mathbf{U}^-=\mathbf{V}^-=\begin{bmatrix} 0 & 0 \\ -1 & 0 \end{bmatrix} , \qquad \text{(A7)}$$

in the basis of $e_u^\pm$ and $e_g^\pm$. The $Q^\pm$ are defined by $Q^\pm=\mp(Q_\theta\pm iQ_\varepsilon)/\sqrt{2}$. The matrix describing the adiabatic potential is then given by

TABLE VI. The intensities for the symmetry allowed transitions from the A_{1g} ground state to the various excited states, obtained by using Eq. (A5). Common factors in the intensity are excluded.

Final state	Intensity
$E_1:E^a_u$	E^2
$E_1:E^b_u$	–
$E_2:A_{2u}$	A^2
$E_2:E_u$	–
$E_3:A^a_{2u}$	A^2
$E_3:A^b_{2u}$	–
$E_4:E^a_u$	E^2
$E_4:E^b_u$	–

$$\begin{bmatrix} E_1 & 0 & 0 & 0 & \frac{V_gQ^+}{\sqrt{2}} & \frac{V_uQ^+}{\sqrt{2}} & \frac{iV_gQ^+}{\sqrt{2}} & \frac{-iV_uQ^+}{\sqrt{2}} \\ 0 & E_1 & 0 & 0 & \frac{-V_gQ^-}{\sqrt{2}} & \frac{-V_uQ^-}{\sqrt{2}} & \frac{iV_gQ^-}{\sqrt{2}} & \frac{-iV_uQ^-}{\sqrt{2}} \\ 0 & 0 & E_4 & 0 & \frac{-V_uQ^+}{\sqrt{2}} & \frac{-V_gQ^+}{\sqrt{2}} & \frac{iV_uQ^+}{\sqrt{2}} & \frac{-iV_gQ^+}{\sqrt{2}} \\ 0 & 0 & 0 & E_4 & \frac{V_uQ^-}{\sqrt{2}} & \frac{V_gQ^-}{\sqrt{2}} & \frac{iV_uQ^-}{\sqrt{2}} & \frac{-iV_gQ^-}{\sqrt{2}} \\ \frac{-V_gQ^-}{\sqrt{2}} & \frac{V_gQ^+}{\sqrt{2}} & \frac{V_uQ^-}{\sqrt{2}} & \frac{-V_uQ^+}{\sqrt{2}} & E_2 & 0 & 0 & 0 \\ \frac{-V_uQ^-}{\sqrt{2}} & \frac{V_uQ^+}{\sqrt{2}} & \frac{V_gQ^-}{\sqrt{2}} & \frac{-V_gQ^+}{\sqrt{2}} & 0 & E_3 & 0 & 0 \\ \frac{iV_gQ^-}{\sqrt{2}} & \frac{iV_gQ^+}{\sqrt{2}} & \frac{iV_uQ^-}{\sqrt{2}} & \frac{iV_uQ^+}{\sqrt{2}} & 0 & 0 & E_2 & 0 \\ \frac{-iV_uQ^-}{\sqrt{2}} & \frac{-iV_uQ^+}{\sqrt{2}} & \frac{-iV_gQ^-}{\sqrt{2}} & \frac{-iV_gQ^+}{\sqrt{2}} & 0 & 0 & 0 & E_3 \end{bmatrix} , \tag{A8}$$

where the E_i's are the unperturbed energies including the elastic energy $m\omega^2(Q_\theta^2+Q_\varepsilon^2)/2$. The electronic basis functions in the JT matrix is $\{\psi_1(E_1^a), \psi_1(E_{-1}^a), \psi_4(E_1^a), \psi_4(E_{-1}^a), \psi_2(A_1), \psi_3(A_1^a), \psi_2(A_2), \psi_3(A_2^a)\}$. The dipole strength could only be transferred among these states and the other four states remain invisible irrespective of the strength of the JT coupling.

In the full treatment of the uniaxial stress perturbation, only the interaction between the $\psi_1(E_1^a)$, $\psi_1(E_{-1}^a)$, $\psi_4(E_1^a)$, $\psi_4(E_{-1}^a)$, $\psi_2(A_1)$, $\psi_3(A_1^a)$, $\psi_2(A_2)$, $\psi_3(A_2^a)$ states has to be considered. All states are assumed to show the same hydrostatic shifts, i.e., the $\mathcal{A}_1$ and $\mathcal{A}_2$ parameters are identical. The x, y, and z directions were chosen to be parallel to $(1,1,-2)/\sqrt{6}$, $(1,-1,0)/\sqrt{2}$, and $(1,1,1)/\sqrt{3}$, respectively. The full stress matrix is then given by

$$\begin{bmatrix} E(A_0) & 0 & 0 & 0 & E_g^- & E_u^- & iE_g^- & iE_g^- \\ 0 & E(A_0) & 0 & 0 & E_g^+ & E_u^+ & -iE_g^+ & iE_u^+ \\ 0 & 0 & E(F_0) & 0 & -E_u^- & -E_g^- & iE_u^- & -iE_g^- \\ 0 & 0 & 0 & E(F_0) & -E_u^+ & -E_g^+ & -iE_u^+ & iE_g^+ \\ E_g^+ & E_g^- & -E_u^+ & -E_u^- & E(B_0) & 0 & 0 & 0 \\ E_u^+ & E_u^- & -E_g^+ & -E_g^- & 0 & E(D_0) & 0 & 0 \\ -iE_g^+ & iE_g^- & -iE_u^+ & iE_u^- & 0 & 0 & E(C_0) & 0 \\ iE_u^+ & -iE_u^- & iE_g^+ & -iE_g^- & 0 & 0 & 0 & E(E_0) \end{bmatrix} \tag{A9}$$

in the same basis as for the JT matrix. The diagonal elements contain both the experimental energies of the lines and the hydrostatic stress shifts as given in Eq. (3a). The off-diagonal elements are defined by

$$\begin{aligned} E_g^+ &= \frac{-(E_g\sigma_- + E_g'\sigma_-')}{\sqrt{2}} , \\ E_g^- &= \frac{(E_g\sigma_+ + E_g'\sigma_+')}{\sqrt{2}} , \\ E_u^+ &= \frac{-(E_u\sigma_- + E_u'\sigma_-')}{\sqrt{2}} , \\ E_u^- &= \frac{(E_u\sigma_+ + E_u'\sigma_+')}{\sqrt{2}} , \end{aligned} \tag{A10}$$

where E_g, E_g', E_u, and E_u' are parameters to be fitted to the experiment and

$$\begin{aligned} \sigma_+ &= \frac{-(\sigma_{yy}-\sigma_{xx}+2i\sigma_{xy})}{\sqrt{2}} , \\ \sigma_- &= \frac{(\sigma_{yy}-\sigma_{xx}-2i\sigma_{xy})}{\sqrt{2}} , \\ \sigma_+' &= \frac{-(\sigma_{xz}+i\sigma_{yz})}{\sqrt{2}} , \\ \sigma_-' &= \frac{(\sigma_{xz}-i\sigma_{yz})}{\sqrt{2}} . \end{aligned} \tag{A11}$$

ACKNOWLEDGMENTS

The authors acknowledge financial support from the Swedish Natural Science Research Council and the Swedish Board for Industrial and Technical Development.

[1] A. Fazzio, M. J. Caldas, and A. Zunger, Phys. Rev. B **32**, 934 (1985).

[2] S. Braun and H. G. Grimmeiss, J. Appl. Phys. **45**, 2658 (1974).

[3] G. D. Watkins, M. Kleverman, A. Thilderkvist, and H. G. Grimmeiss, Phys. Rev. Lett. **67**, 1149 (1991).

[4] L-Å. Ledebo and Z-G. Wang, Appl. Phys. Lett. **42**, 680 (1983).

[5] D. Thebault, J. Barrau, G. Armelles, N. Lauret, and J. P. Noguier, Phys. Status Solidi B **125**, 357 (1984).

[6] M. Kleverman, J. Olajos, and H. G. Grimmeiss, Phys. Rev. B **35**, 4093 (1987).

[7] J. W. Petersen and J. Nielsen, Appl. Phys. Lett. **56**, 1122 (1990).

[8] M. Kleverman, J. Olajos, and H. G. Grimmeiss, *Proceedings of the International Conference on the Physics of Semiconductors,* edited by E. M. Anastassakis and J. D. Joannopoulos (World Scientific, Singapore, 1990), p. 541.

[9] K. Ohta, Sci. Light (Tokyo) **22**, 12 (1973).

[10] C. Cohen-Tannoudji, B. Diu, and F. Laloe, *Quantum Mechanics* (Wiley, New York, 1977).

[11] A. E. Huges and W. A. Runciman, Proc. Phys. Soc. **90**, 827 (1967).

[12] A. A. Kaplyanskii, Optika Spectrosk. **16**, 602 (1964) [Opt. Spectrosc. (USSR) **16**, 329 (1964)].

[13] G. D. Watkins, Physica B **117**, 9 (1983); **118**, 9 (1983).

[14] G. D. Watkins and J. W. Corbett, Phys. Rev. A **138**, 543 (1985).

[15] A. Abragam and B. Bleaney, *Electron Paramagnetic Resonance of Transition Ions* (Dover, New York, 1986).

[16] G. F. Koster, J. O. Dommock, R. G. Wheeler, and H. Statz, *Properties of the Thirty-Two Point Groups* (MIT, Cambridge, Massachusetts, 1963).